2018 IEEE International Conference on Robotics and Automation (ICRA)
May 21-25, 2018, Brisbane, Australia

# Autonomous Control of the Interacting-BoomCopter UAV for Remote Sensor Mounting

Daniel R. McArthur, Arindam B. Chowdhury, and David J. Cappelleri

*Abstract*— **This paper presents a novel approach for autonomously mounting a sensor package on a vertical surface with an unmanned aerial vehicle (UAV). The Interacting-BoomCopter (I-BC) UAV uses an on-board webcam and computer along with a horizontally-mounted reversible propeller on its front boom to autonomously perform the aerial manipulation task. An overview of the vehicle design is presented along with the image processing algorithms used for target tracking, and the implementation of an extended finite state machine (EFSM) for carrying out the high-level autonomous control. The effectiveness of the autonomous control strategy and I-BC platform are examined through the performance of several autonomous sensor mounting flight tests.**

## I. INTRODUCTION

In recent years, there has been a significant increase in the use of unmanned aerial vehicles (UAVs) in various applications, including precision agriculture, mapping, inspection, surveillance, and construction. In these applications, the UAV is used primarily for data collection and image transmission. However, with advances in light-weight computing and battery technologies, a new trend is emerging to use UAVs to interact physically with the environment. This trend shows great promise in applications where humans are required to perform dangerous or time-consuming tasks in hard-to-reach places. One such application is the inspection and maintenance of the infrastructure that forms our utility, communication and transportation networks. Structures such as bridges, cell towers, power lines, and nuclear reactors, require regular inspection and maintenance to ensure structural integrity and prevent leaks, spills and even disasters. The completion of these tasks by humans is hindered by accessibility and safety concerns and human limitations in consistency and efficiency. Many structures (such as bridges and towers) have regions that are inaccessible without expensive closures and/or the use of costly equipment. Furthermore, aging infrastructure and natural disasters generate a continuous demand for inspection and maintenance and place strict constraints on the time allotted for the completion of these tasks. There is great potential for new UAV platforms to help overcome many of these limitations. These UAV platforms must be endowed with unique capabilities including the ability to carry multiple sensing payloads (such as cameras and distance sensors), and the ability to interact with the environment for tasks such as applying sealants, marking areas of interest, cleaning joints, placing remote sensors, etc.

The authors are with the School of Mechanical Engineering, Purdue University, West Lafayette, IN 47907, USA. {dmcarth, abhanjac, dcappell}@purdue.edu This is based upon work supported by the National Science Foundation Graduate Research Fellowship Program under Grant No. DGE-1333468. Any opinions, findings, and conclusions or recommendations expressed in this material are those of the author(s) and do not necessarily reflect the views of the NSF.


Fig. 1. Interacting-BoomCopter (I-BC) UAV prototype equipped for remote sensor mounting.

Recent research efforts have considered various types of physical interaction capabilities for UAVs: transportation and delivery [1], [2], [3], object manipulation [4], [5], [6], [7], [8], [9], [10], assembly [11], and contact inspection tasks [12], [13], [14]. Due to the potential instabilities introduced by physical interactions with the environment, a UAV with stable hovering capabilities is desired, such as a vertical takeoff and landing (VTOL) platform. However, typical VTOL platforms are underactuated, i.e. have fewer actuators than degrees-of-freedom. This limits their ability to perform aerial manipulation tasks that require the vehicle to resist or apply arbitrary forces and torques. A number of fully or overly-actuated multirotor platforms have recently been developed to accomplish these types of tasks: quadrotors with tilting [15], [16], [17] or horizontally mounted propellers [18]; hex-rotor platforms [19], [20], [21]; an eight-propeller configuration [22]; and one that combines counter-rotating propellers and variable angle ducted fans [23]. In a similar effort, we presented the design of the Interacting-BoomCopter (I-BC) UAV in our previous work [24], [25]. The I-BC is a tri-rotor VTOL aircraft with a horizontally-mounted, reversible propeller on the front boom which generates pushing and pulling forces for interacting with the environment (Fig. 1).

In this paper, we consider and describe a representative autonomous interaction task for the I-BC associated with inspection and maintenance activities. Next, a brief overview of the I-BC vehicle design is provided, followed by a description of the designed autonomous control strategy that allows the I-BC to interact with the environment in an accurate and repeatable way. Finally, the results of several autonomous experimental flight tests are presented and discussed.

## II. INTERACTION TASK OVERVIEW

There are many tasks such as structural health monitoring, air quality assessment, general surveillance, etc. that require sensors or markers to be placed in remote or high-up locations. As such, we consider here the representative task of remotely mounting a sensor on a vertical surface and develop image processing and autonomous control strategies for the I-BC. For this task, we designed a small sensor package in [25] which houses a wireless surveillance camera, but the same form factor ($3.1\ cm \times 5.1\ cm \times 5.8\ cm$, mass $< 100\ g$) could easily house a number of other sensors including vibration, temperature, or air quality sensors, etc. In this work, our goal is to autonomously mount the sensor package at a specific location on a vertical surface using a visual marker on the vertical surface as a reference point.

## III. VEHICLE DESIGN OVERVIEW

The Interacting-BoomCopter (I-BC) UAV is a tri-copter with an additional arm extending out the front (the front boom) that is used to perform aerial manipulation tasks. A thorough description of the I-BC's vehicle design and dynamic model is provided in [24] and [25]. The I-BC's key components are labeled in Fig. 1 and a brief design overview is provided below.

### A. On-board Sensors and Computers

A Pixhawk flight control unit (FCU) with PX4 Firmware stabilizes and controls the vehicle's attitude and position during flight. The FCU also provides an "Offboard" flight mode that allows an external computer to command the vehicle's position and heading (yaw angle). These commands are generated in-flight by an Odroid XU4 single board computer based on feedback from on-board image, force, and distance sensors. An Arduino Pro Mini microcontroller reads the force and distance sensor values and forwards them to the XU4 for further processing.

### B. Boom Propeller Design

Pushing and pulling forces are generated in the horizontal plane by the boom propeller (boom-prop): a reversible, 4-blade propeller mechanism mounted on the front boom. Fig. 2(a) shows an exploded view of the boom-prop assembly. The boom-prop uses reversible (3D) propeller blades that generate the same amount of thrust when rotated clockwise or counter-clockwise (as opposed to traditional propellers that are optimized to generate thrust when rotated in a particular direction). This allows the I-BC to transition from pushing to pulling strictly through software, by inverting the command sent to the reversible electronic speed controller (ESC). The orientation of the boom-prop in-line with the vehicle center of gravity allows the I-BC to move forward and in reverse without pitching. This is advantageous when interacting with the environment, since the I-BC can operate at or near its most stable hovering configuration during all stages of the interaction.

### C. Push-To-Release End-Effector Design

Several lightweight, modular end-effectors have been designed to interact with the environment by utilizing the pushing and pulling forces generated by the I-BC's boom-prop. One of these end-effectors, shown in Fig. 2(b), employs a passive push-to-release-mechanism (PTRM) that can be used to mount a sensor package on a vertical surface. The PTRM consists of a main body attached to the I-BC by a slide rail and a detachable knob that is permanently affixed to a sensor package. Before takeoff, the sensor package (with knob affixed) is pressed into the PTRM housing and locked in place. When the I-BC uses its boom-prop to press the sensor package against a vertical surface, the knob slides into the PTRM housing and toggles the mechanism to release the knob. Very high bond double-sided tape on the back of the sensor keeps it in place on the vertical surface as the I-BC pulls away. Since the PTRM slides freely on a slide rail, all of the pushing force applied to the sensor package is transmitted in series to the force sensor on the end-effector, thus allowing for force feedback during sensor mounting operations. A sonar sensor mounted above the PTRM also provides precise distance measurements from the end-effector to the vertical surface, allowing for finer depth control during the approach to and retreat from the mounting surface.

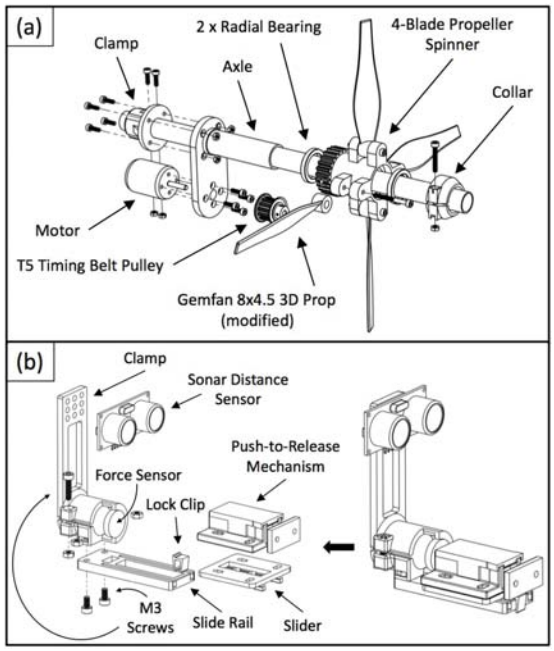


Fig. 2. Vehicle design overview. (a) Boom propeller assembly; (b) Push-to-release end-effector assembly.

## IV. AUTONOMOUS CONTROL

During normal flight, the Pixhawk flight control unit (FCU) on the I-BC operates in one of several flight modes (e.g. stabilize attitude, altitude control, position control, etc.). The I-BC's remote controller (RC) is programmed to allow the pilot to use physical switches to change the FCU's flight mode and turn the boom-prop on or off as desired. Previous work [25] has shown that, with this setup, a pilot can teleoperate the I-BC to remotely mount a sensor package on a wall. This is done by manually flying the I-BC to a desired altitude, switching the FCU to altitude control mode, positioning the vehicle in front of the target position, switching on the boom-prop until the sensor is mounted on the wall, then reversing or switching off the boom-prop and returning to a safe position

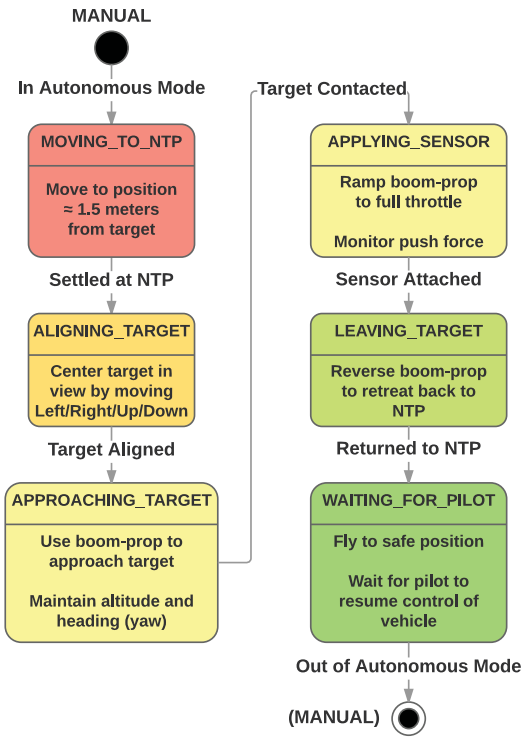


Fig. 3. State-transition diagram for autonomous sensor mounting task.

to land. As expected, the accuracy and repeatability of this manual sensor placement are highly dependent on the pilot's skill level and the amount of attention that the pilot can safely allocate to the task while maintaining stable flight and a sufficient awareness of the vehicle's surroundings. Thus, a software package was developed to perform the sensor mounting task autonomously. The software uses feedback from the on-board webcam and force and distance sensors to ensure that the task is performed safely and accurately.

### A. Extended Finite State Machine

The autonomous sensor mounting task consists of several operations performed sequentially, and is ideally suited for implementation in software as an extended finite state machine (EFSM). Each operation to be performed corresponds to a state in the EFSM, and state transitions are triggered by various events (e.g. when the I-BC arrives at a desired position). Fig. 3 shows the state-transition diagram for the sensor mounting task. Note that, for safety purposes, the pilot can enable or disable the autonomous controller at any time by toggling a switch on the RC, and fail-safes triggered by logical error conditions or sensor failures also return control to the pilot immediately.

*1) Moving to Near-Target Position:* It is assumed that the precise location where the sensor will be mounted, referred to as the target position (TP), is unknown prior to takeoff. Thus, the initial state (shown in red in Fig. 3) brings the vehicle to a near-target position (NTP) that is within 1-2 meters of the desired TP. Experimentally, the NTP is defined with a workspace coordinate in a Vicon motion capture volume used for testing. In application, the NTP could be specified by a GPS coordinate near the TP, or the pilot could manually fly to this position based on direct line-of-sight operation or with feedback from the on-board webcam video stream. The NTP also specifies a heading angle which ensures that the vehicle's forward axis (body X axis) is perpendicular to the mounting surface. As the I-BC moves to its commanded position and heading setpoint, the EFSM compares its current estimated position with the setpoint, and triggers an event after the vehicle stays within a small envelope ($\leq 10cm$) in each direction of the setpoint for a predetermined amount of time. Once at the NTP, the I-BC adjusts its perpendicular distance to the wall (based on the forward-facing sonar readings) to ensure an optimal field of view for target tracking with the webcam.

*2) Aligning Vehicle with Target:* With the vehicle stationed at a position near the mounting surface and within view of the TP, the EFSM transitions to the `ALIGNING_TARGET` state (shown in orange in Fig. 3). In this state, the TP is estimated by fusing the object tracking data from the webcam with the sonar distance readings and the vehicle pose estimate. The error due to time delay between the webcam image capture and the most recent pose estimate is minimal due to the high update rate of the pose estimate (100 Hz).

The object tracking algorithm can track either a predefined visual target, or a target specified by the user clicking in the live video feed from the I-BC's webcam. More details on this algorithm are provided in Sec. IV-B. Once an estimate of the TP is available, the I-BC's position setpoint is adjusted so that the end-effector is aligned horizontally and vertically with the TP. This position setpoint is referred to as the Webcam-Tuned NTP.

*3) Mounting Sensor and Retreating:* Once the vehicle has arrived at the Webcam-Tuned NTP, it is positioned directly in front of the desired mounting location and the EFSM transitions into the `APPROACHING_TARGET` state. The desired approach trajectory is computed by forming a 3D line between the Webcam-Tuned NTP and the TP. The boom-prop is then ramped up to $\approx 20\%$ throttle to move the vehicle forward along the desired trajectory. During the approach, the vehicle's position setpoint is continuously updated by projecting the current vehicle position onto the desired approach trajectory. This allows the position controller to correct horizontal and vertical deviations from external disturbances (e.g. wind) while simultaneously preventing it from commanding non-zero pitch angles, since the forward motion is generated by the boom-prop.

The force sensor in series with the sensor package is used to determine when the package comes into contact with the mounting surface. When the detected pushing force exceeds a predetermined threshold, a collision event is triggered and the EFSM transitions to the `APPLYING_SENSOR` state. At this point, the boom-prop is ramped up to full throttle while the force sensor data is monitored to ensure that the sensor package is pressed firmly in place and that the PTRM toggles to release the sensor package. After the sensor package is in place, the EFSM transitions to the `LEAVING_TARGET` state and the boom-prop throttle is

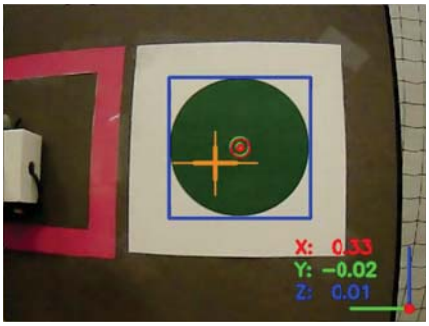


Fig. 4. Green pattern used to estimate the position of the I-BC. The bounding blue rectangle and red center point are used to calculate the distance from the pattern. The orange crosshairs indicate the center of the webcam frame. The numbers are the x, y and z distances from the center of the webcam frame (crosshairs) to the center of the pattern (red dot). The X-axis is directed into the page, the Y-axis is to the left, and the Z-axis is directed upwards.

reversed to $\approx -20\%$ to move the I-BC away from the wall and back to the Webcam-Tuned NTP (the initial position of the `APPROACHING_TARGET` state). At this point, the EFSM transitions to its final state, and the I-BC holds its position until the pilot resumes manual control.

### B. Real-time Image Processing

As stated above, the EFSM utilizes real-time image processing from the on-board webcam to align the vehicle with the target. This approach is chosen since it works well for both indoor and outdoor environments and there are a multitude of powerful lightweight cameras available today [26]. We use a green circular pattern (placed next to the TP on the wall) to localize the I-BC for this particular task. Our image processing algorithm is divided into two phases: pattern detection and position estimation, which are described below. A simple algorithm for the pattern detection is used in order to reduce the computational burden on the on-board computer. The algorithm uses OpenCV 3 and runs at $\approx 20$ Hz on the on-board computer.

*1) Pattern Detection:* When the algorithm starts up, the live webcam image feed is sent from the I-BC to a laptop so that the user can select the (green) color pattern and initialize the algorithm. Once the color pattern is clicked, the algorithm running on the I-BC's on-board computer calculates the Hue-Saturation-Value (HSV) of the selected pixel and uses these values to filter the subsequent webcam video frames. Therefore, the ensuing image frames only show objects with HSV color values within a small threshold of the selected pixel. Thus, the pattern is detected (in the absence of any other similarly-colored objects). A blue rectangle is then drawn around the detected pattern, as shown in Fig. 4.

As the I-BC changes position, the pattern will appear bigger or smaller, depending on the distance from the target. Due to these changes and the variability in lighting conditions, the initial HSV values used as thresholds for the filter may no longer be valid. Therefore, the algorithm dynamically updates the threshold values for the color filter. Every time it detects the pattern, the HSV values of the pixels at the centroid of the patten are used as the filter thresholds for the next iteration.

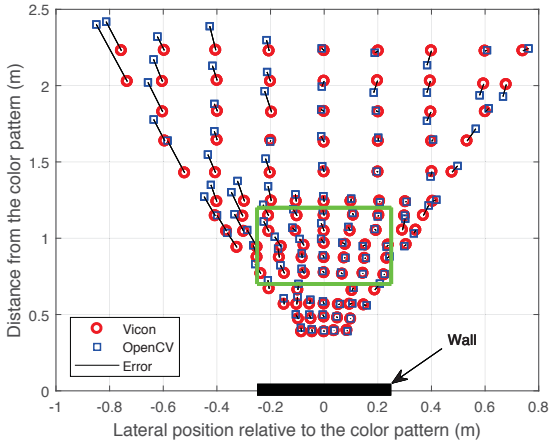


Fig. 5. Top view of the experimental room. Map of actual position obtained from the Vicon system and estimated position calculated from OpenCV. Estimation error increases further away from the pattern. Thus, we utilize the on-board camera for position estimates only when the I-BC is within the green rectangular zone (0.7 to 1.2 $m$ away from the wall).

*2) Position Estimation:* Once the pattern has been detected, the position estimate of the I-BC relative to the TP needs to be determined. The on-board attitude controller ensures that the I-BC stays perpendicular to the wall and performs only negligible yaw movements during the position estimation routine. The sonar sensor mounted to the end-effector is used to measure the distance to the TP (wall) while the position of the tracked color pattern in the image is used to determine the relative position between the I-BC and TP and compute movement commands in the Y- (left, right) and Z-axes (up, down) to align the I-BC with the target (Fig.4). The position of the tracked color pattern is initially computed in pixels relative to the center of the image frame. Therefore, the appropriate scale to convert from pixel values to a distance value in meters is needed. We make use of the known size (area) of the colored circle (10 $cm$ diameter) and compare it with the corresponding pixel value in the image to make this conversion. To check the accuracy of this routine, we placed the I-BC at different distances from the wall, measured the exact distance using the Vicon motion capture cameras, and recorded the size of the pattern as seen through the webcam (see Fig.5). The area of the pattern decreases nonlinearly as the distance from the pattern increases. Fitting an exponential curve to this data gives us an estimate of the distance to the wall as a function of the pattern area (with an error of about $\pm 4$ $cm$), and the corresponding pixel-to-meter scale factor. Based on these values, the I-BC is commanded to move laterally and vertically to align the center of the image with the center of the color pattern.

The EFSM only uses the image processing algorithm to determine position estimates for control if the I-BC is within the highlighted region shown in Fig.5. This ensures that the green pattern is within the camera's field of view and that the estimation errors are low.

## V. EXPERIMENTAL RESULTS

We performed several flight tests to experimentally validate the performance of the autonomous control algorithm

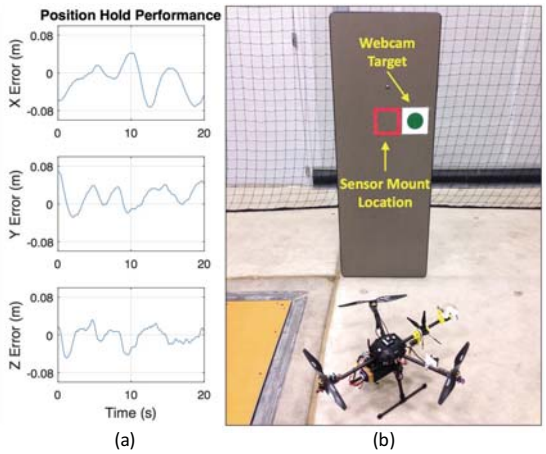


Fig. 6. (a) Performance of I-BC's FCU position controller. (b) Experimental setup for an autonomous sensor mounting task. The red square is centered on the desired mounting location (TP), and the width of the square (16 $cm$) indicates the acceptable placement error. The green circle is tracked by the webcam. Table dimensions: 0.61 x 1.68 $m$.

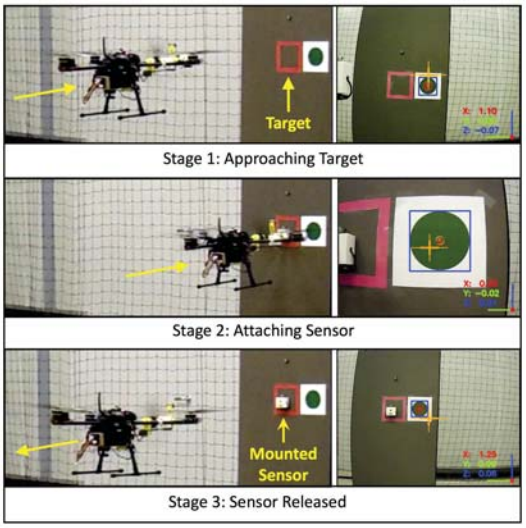


Fig. 7. Video screenshots from a successful autonomous sensor mounting operation. Right Column: view from on-board webcam.

discussed in the previous section. Since the vehicle's 3D position and heading are controlled by the FCU during both manual and autonomous flight, the sensor mounting performance is dependent on the performance of the FCU position controller and the general stability of the airframe. After tuning the position controller gains to optimize the vehicle's response time and minimize positioning error, we determined that the I-BC's position can be reliably maintained within about $\pm 8$ $cm$ of the position setpoint (see Fig. 6(a)).

### A. Experiment Setup

Fig. 6(b) shows the experimental test setup in the lab. A table turned on end was used as a rigid mounting surface ($0.61$ $m$ $\times$ $1.68$ $m$ tall). The use of this table simulates scenarios where the width of the desired mounting surface is constrained (e.g. mounting a sensor on a truss member), but we assume that the results from the experiments are also applicable to scenarios with larger mounting surfaces such as walls. As discussed in Section IV-B above, the green circle ($10$ $cm$ diameter) was used as a tracking target for the image processing algorithm. The red square outline indicates the desired sensor mounting location (TP) and the acceptable positioning error (due to the limitations of the airframe/FCU). Any sensor placement inside or on the edge of the red outline is considered successful. In our experiments, the green target was offset to the right of the actual mounting location for convenience in measuring the sensor placement performance, and so that the sensor adhesive is attached to the actual mounting surface and not the printed paper target.

### B. Sensor Placement Performance

Out of 15 total flights, 11 resulted in a successful autonomous sensor mount, and 4 flights were aborted prematurely due to fail-safes. Fig. 7 shows the sensor mounting operation from both external and on-board viewing angles. When evaluating the sensor placement performance, we considered comparisons of the target mounting location (TP) against both the estimated mounting location (based on image processing) and the actual mounting location. As expected, the image processing estimation and actual sensor placement error each varied randomly between trials. Fig. 8 shows the absolute error in the estimated and actual sensor mounting locations for each of the 11 successful flight tests. The maximum overall placement error from the test flights was $9.3$ $cm$ and the average error was $6.3$ $cm$.

During the autonomous sensor mounting process, the EFSM calculates various position setpoints to maneuver the I-BC to the mounting position. Fig. 9 shows these setpoints (red squares) along with the I-BC's travel path for one of the successful autonomous sensor mounting flights. The force applied to the sensor during impact on the same flight is also included as an inset in Fig. 9.

The original EFSM design used two states to apply the sensor (shown in yellow in Fig. 3). However, we found in our experiments that the initial impact and resulting bounce-back of the I-BC from the wall caused the sensor package to be released from the PTRM and remain on the wall. Thus, we modified the `APPROACHING_TARGET` state to transition directly to the `LEAVING_TARGET` state a short time ($\approx 0.75$ $s$) after detecting the impact with the wall. Our future work will address adding compliance to the end-effector to limit/remove bounce-back during actual sensor placement.

## VI. CONCLUSIONS

In this paper, we have presented an autonomous control strategy that enables remote sensor placement with the I-BC UAV. To demonstrate this capability, we performed several successful flight tests in which a wireless surveillance camera package was mounted at a target location on a vertical surface. In these tests, the I-BC used feedback from an on-board webcam to localize itself relative to the target mounting location in real time, and repeatably placed the sensor at the desired location. Future work will incorporate more sophisticated image processing algorithms to enable real-time tracking of more complex visual reference features

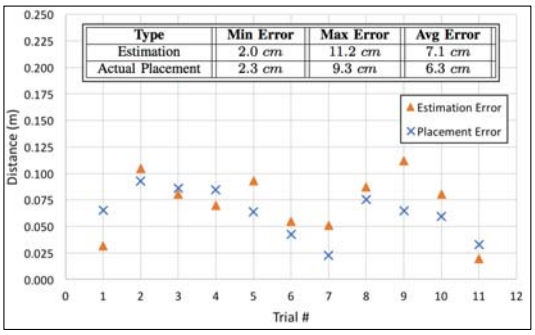


Fig. 8. Image processing estimate error and sensor placement error relative to ground truth (Vicon) for 11 test flights. Inset table lists minimum, maximum and average errors across all trials.

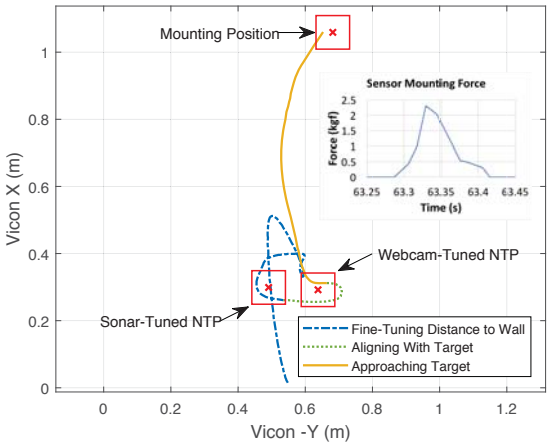


Fig. 9. Top view of I-BC position during sensor mounting task. Red squares indicate autonomously calculated position setpoints. Inset: Force on sensor package during impact.

(e.g. a bolt pattern on a structure) and improve upon the end-effector design to help stabilize the dynamic interactions with the mounting surface.

## REFERENCES


[1] D. Mellinger, M. Shomin, N. Michael, and V. Kumar, *Cooperative Grasping and Transport Using Multiple Quadrotors*. Berlin, Heidelberg: Springer Berlin Heidelberg, 2013, pp. 545–558.

[2] P. O. Pereira and D. V. Dimarogonas, "Stability of load lifting by a quadrotor under attitude control delay," in *2017 IEEE International Conference on Robotics and Automation (ICRA)*, May 2017, pp. 3287–3292.

[3] A. Gawel, M. Kamel, T. Novkovic, J. Widauer, D. Schindler, B. P. von Altishofen, R. Siegwart, and J. Nieto, "Aerial picking and delivery of magnetic objects with mavs," in *2017 IEEE International Conference on Robotics and Automation (ICRA)*, May 2017, pp. 5746–5752.

[4] D. Mellinger, Q. Lindsey, M. Shomin, and V. Kumar, "Design, modeling, estimation and control for aerial grasping and manipulation," in *2011 IEEE/RSJ International Conference on Intelligent Robots and Systems*, Sept 2011, pp. 2668–2673.

[5] R. Mebarki, V. Lippiello, and B. Siciliano, "Toward image-based visual servoing for cooperative aerial manipulation," in *2015 IEEE International Conference on Robotics and Automation (ICRA)*, May 2015, pp. 6074–6080.

[6] F. Huber, K. Kondak, K. Krieger, D. Sommer, M. Schwarzbach, M. Laiacker, I. Kossyk, S. Parusel, S. Haddadin, and A. Albu-Schäffer, "First analysis and experiments in aerial manipulation using fully actuated redundant robot arm," in *2013 IEEE/RSJ International Conference on Intelligent Robots and Systems*, Nov 2013, pp. 3452–3457.

[7] M. Fumagalli, R. Naldi, A. Macchelli, F. Forte, A. Q. L. Keemink, S. Stramigioli, R. Carloni, and L. Marconi, "Developing an aerial manipulator prototype: Physical interaction with the environment," *IEEE Robotics Automation Magazine*, vol. 21, no. 3, pp. 41–50, Sept 2014.

[8] K. Kondak, K. Krieger, A. Albu-Schaeffer, M. Schwarzbach, M. Laiacker, I. Maza, A. Rodriguez-Castano, and A. Ollero, "Closed-loop behavior of an autonomous helicopter equipped with a robotic arm for aerial manipulation tasks," *International Journal of Advanced Robotic Systems*, vol. 10, no. 145, 2013.

[9] M. Manubens, D. Devaurs, L. Ros, and J. Cortés, "Motion planning for 6-d manipulation with aerial towed-cable systems," in *Proceedings of Robotics: Science and Systems*, Berlin, Germany, June 2013.

[10] M. Orsag, C. Korpela, and P. Oh, "Modeling and control of mm-uav: Mobile manipulating unmanned aerial vehicle," *Journal of Intelligent & Robotic Systems*, vol. 69, no. 1, pp. 227–240, 2013.

[11] F. Augugliaro, A. Mirjan, F. Gramazio, M. Kohler, and R. D'Andrea, "Building tensile structures with flying machines," in *2013 IEEE/RSJ International Conference on Intelligent Robots and Systems*, Nov 2013, pp. 3487–3492.

[12] T. Bartelds, A. Capra, S. Hamaza, S. Stramigioli, and M. Fumagalli, "Compliant aerial manipulators: Toward a new generation of aerial robotic workers," *Robotics and Automation Letters, IEEE*, vol. 1, no. 1, pp. 477–483, January 2016.

[13] K. Alexis, C. Huerzeler, and R. Siegwart, "Hybrid modeling and control of a coaxial unmanned rotorcraft interacting with its environment through contact," in *Robotics and Automation (ICRA), 2013 IEEE International Conference on*, May 2013, pp. 5417–5424.

[14] L. Marconi, R. Naldi, and L. Gentili, "Modeling and control of a flying robot interacting with the environment," *Automatica*, vol. 47, no. 12, pp. 2571 – 2583, 2011. [Online]. Available: http://www.sciencedirect.com/science/article/pii/S0005109811004602

[15] M. Ryll, H. H. Bülthoff, and P. R. Giordano, "Modeling and control of a quadrotor uav with tilting propellers," in *Robotics and Automation (ICRA), 2012 IEEE International Conference on*, May 2012, pp. 4606–4613.

[16] A. Oosedo, S. Abiko, S. Narasaki, A. Kuno, A. Konno, and M. Uchiyama, "Flight control systems of a quad tilt rotor unmanned aerial vehicle for a large attitude change," in *2015 IEEE International Conference on Robotics and Automation (ICRA)*, May 2015, pp. 2326–2331.

[17] C. Papachristos, K. Alexis, and A. Tzes, "Efficient force exertion for aerial robotic manipulation: Exploiting the thrust-vectoring authority of a tri-tiltrotor uav," in *2014 IEEE International Conference on Robotics and Automation (ICRA)*, May 2014, pp. 4500–4505.

[18] A. Albers, S. Trautmann, T. Howard, T. A. Nguyen, M. Frietsch, and C. Sauter, "Semi-autonomous flying robot for physical interaction with environment," in *2010 IEEE Conference on Robotics, Automation and Mechatronics*, June 2010, pp. 441–446.

[19] G. Jiang and R. Voyles, "Hexrotor uav platform enabling dextrous interaction with structures-flight test," in *2013 IEEE International Symposium on Safety, Security, and Rescue Robotics (SSRR)*, Oct 2013, pp. 1–6.

[20] E. Kaufman, K. Caldwell, D. Lee, and T. Lee, "Design and development of a free-floating hexrotor uav for 6-dof maneuvers," in *2014 IEEE Aerospace Conference*, March 2014, pp. 1–10.

[21] S. Rajappa, M. Ryll, H. H. Bülthoff, and A. Franchi, "Modeling, control and design optimization for a fully-actuated hexarotor aerial vehicle with tilted propellers," in *2015 IEEE International Conference on Robotics and Automation (ICRA)*, May 2015, pp. 4006–4013.

[22] D. Brescianini and R. D'Andrea, "Design, modeling and control of an omni-directional aerial vehicle," in *2016 IEEE International Conference on Robotics and Automation (ICRA)*, May 2016, pp. 3261–3266.

[23] Y. Long, L. Wang, and D. J. Cappelleri, "Modeling and global trajectory tracking control for an over-actuated mav," *Advanced Robotics*, vol. 28, no. 3, pp. 145–155, 2014.

[24] D. R. McArthur, A. B. Chowdhury, and D. J. Cappelleri, "Design of the i-boomcopter uav for environmental interaction," in *2017 IEEE International Conference on Robotics and Automation (ICRA)*, May 2017, pp. 5209–5214.

[25] ——, "Design of the i-boomcopter uav for remote sensor mounting," in *ASME 2017 IDETC/CIE, International Design Engineering Technical Conferences & Computers and Information in Engineering Conference (IDETC/CIE)*, August 2017.

[26] F. J. Perez-Grau, R. Ragel, F. Caballero, A. Viguria, and A. Ollero, "Semi-autonomous teleoperation of uavs in search and rescue scenarios," in *2017 International Conference on Unmanned Aircraft Systems (ICUAS)*, June 2017, pp. 1066–1074.